Journal of Electron Spectroscopy and Related Phenomena 249 (2021) 147070

Contents lists available at ScienceDirect

Journal of Electron Spectroscopy and Related Phenomena

journal homepage: www.elsevier.com/locate/elspec

Angular distribution and energy spectra of photoelectrons from tetrahydrofuran illuminated by VUV photon source

István Márton [a,*], Levente Ábrók [a,b], Dávid Nagy [a,b], Ákos Kövér [a], László Gulyás [a], Sándor Demes [a], Sándor Ricz [a,1]

[a] Institute for Nuclear Research, (Atomki), P.O. Box 51, H-4001 Debrecen, Hungary
[b] Doctoral School of Physics, University of Debrecen, Egyetem sqr. 1, H-4032 Debrecen, Hungary

A B S T R A C T

Photoelectron emission from the valence shell of biologically relevant tetrahydrofuran (THF) molecule is studied. Energy and angular distributions of photoelectrons from THF ionized by a He(I) vacuum ultraviolet (VUV) photon source are measured. Theoretical calculations performed for the binding energies of orbitals and photoelectron intensities are in reasonable agreement with measurement. The observed angular distributions show the determining role of dipole transition mechanism.

1. Introduction

The radiation damage of DNA molecule is an actively studied field [1,2] which is largely justified by the increasing importance of cancer therapy. To better understand the radiation damage in biological and other materials we need to study the photon, ion and electron (including secondary electrons produced through primary ionization) interactions with atoms and molecules. One way to get detailed information on the processes is to measure the energy and angular distributions of electrons emitted during the collision. For simulation of DNA-damages, e.g. on a level of cellular and subcellular scales, a detailed knowledge of the atomic and molecular properties of the target is needed. High energy resolution angle-resolved spectroscopy (HR-ARPES) together with narrow bandwidth of He(I) vacuum ultraviolet (VUV) radiation is one of the sensitive methods for investigating the dynamical aspect of the ionization process such as electron correlation, multipole and channel interactions, etc.

Tetrahydrofuran (THF, C_4H_8O) can be used as a model molecule representing the deoxyribose group in DNA backbone and therefore there is significant interest towards it [3–5]. The total ionization cross sections of THF have been investigated previously both with electron and positron impacts [6]. There is also a broad literature aimed at the investigation of the properties of excitation and ionization processes of THF induced either by electron collision [7–16] or by photoionization [17–22]. The fragmentation of THF was also investigated by ionizing radiation [10,20]. It was also discovered that secondary electrons induced by ionizing radiation with energies well below the ionization threshold can cause strand breaks in the DNA [23]. This shows the importance of the properties of photoelectron emission from THF. Although there are numerous research carried out to obtain the electron energy spectra of THF, to the best of our knowledge no experiment has been carried out where the angular distribution of the photoelectrons were also measured.

The THF is not a planar but a puckered molecule which has 4 conformational isomers described by the C_1, C_2, C_s and the C_{2v} point groups [24,25]. The most populated conformer of THF was identified as the C_s conformer measured with electron momentum spectroscopy [26]. According to recent studies [16] 45% of THF are C_s isomer meanwhile 55% belongs to the C_2 isomer. Another group [18] concluded that at room temperature ($T = 298$ K) the C_s and C_2 isomers are accounting for the 44.5% and 55.5% of THF respectively.

In this work, we focus on the photoionization of THF induced by He(I) VUV irradiation. Energy and angular distributions of inner and outer valence shell photoelectrons are measured and compared with other available experimental results. Up to our knowledge no previous experimental study was aimed to measure the angular distribution and energy spectrum of THF simultaneously. Theoretical calculation for the process is also performed. Atomic units are used, if otherwise is stated.

2. Experimental setup

Energy and angular distributions of photoelectrons are measured using our unique electrostatic electron spectrometer (ESA-22) [27]. ESA-22 consists of a spherical (SMA) and a cylindrical mirror analyzer (CMA) and is able to detect electrons with energy selected in the 2 eV–10 keV energy range over the entire angular range in a single run.

* Corresponding author.
E-mail address: marton.istvan@atomki.hu (I. Márton).
[1] Deceased author.

https://doi.org/10.1016/j.elspec.2021.147070
Received 8 January 2021; Received in revised form 29 March 2021; Accepted 7 April 2021
Available online 15 April 2021

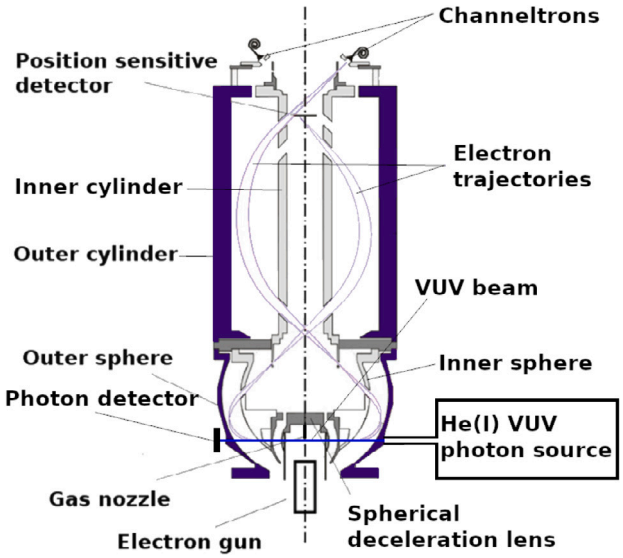

Fig. 1. Experimental setup of the electron spectroscopic analyzer (ESA-22).

The experimental setup is shown in Fig. 1. THF molecules in gas phase are injected to the collision region through a gas nozzle, where they are ionized by photons with 21.218 eV provided by the He(I) vacuum ultraviolet photon source. Electrons ejected from THF molecules are extracted from the collision region and transported to the CMA by a spherical mirror lens. Applying different voltages on the analyzer (SMA, CMA) makes it possible to deliver electrons at different energies to the detectors and therefore the electron energy spectrum can be measured. The electrons are detected by 24 channel electron multipliers (CEM) corresponding to electron trajectories on the left side depicted in Fig. 1. Each CEM is placed on a round holder 15° apart each other. This layout enables us to measure the angular distribution of the electrons in the $0° - 360°$ angular region, simultaneously. The detection angle of a CEM is 1.7° vertically and 3.5° horizontally. The relative energy resolution of the spectrometer is 2.5×10^{-3}.

The UV lamp used in the experiment emits both linearly and circularly polarized light in almost the same proportion. The intensity of the incident photons is measured by a photon detector consisting of an electrically grounded metal plate and an electric current meter with high sensitivity. The VUV photons induce photoemission from the metal surface. This results an electric current between the plate and the ground which is proportional to the VUV photon intensity. The pressure in the vacuum chamber was in the order of 10^{-5} mbar with gas inlet during the measurement and about 10^{-7} mbar without gas. A 3 mm thick μ-metal layer is mounted in the chamber to reduce the Earth's magnetic field resulting in less than 5 mG in the analyzer.

The geometry of the measurement is defined as follows: the z-axis of the coordinate system is pointed into the propagation of the photon beam, while the x-z plane is fixed by the plane of linear polarization. Momentum of the photoelectrons are denoted by $\mathbf{k}_e = (k_e, \theta_e, \phi_e)$. Electrons leaving the collision region are detected only in the x-z plane in the present experiment. Namely distribution of electrons emitted with k_e ($E_e = 1/2k_e^2 \geq 2$ eV), $\theta_e = 90°$ and $-180^o \leq \phi_e \leq 180°$, are observed.

3. Theoretical calculations

The interaction of photon, possessing wave vector $\mathbf{k}$, polarization vector $\mathbf{e}_{\mathbf{k}\lambda}$ (λ=1,2) and angular frequency $\omega_{\mathbf{k}}$, with an electron is described by the operator

$$V_{int} = -\frac{e}{m}\sqrt{\frac{2\pi\hbar}{\omega_{\mathbf{k}} V}}(\mathbf{e}_{\mathbf{k}\lambda} \cdot \mathbf{p})\mathbf{e}^{\mathbf{ik}\cdot\mathbf{r}}, \tag{1}$$

where e and m are, respectively, the charge and mass of an electron, $\mathbf{r}$ and $\mathbf{p} = -i\hbar\nabla$ are, respectively, the position vector and the momentum operator of the electron [28]. In the dipole approximation the expansion

$$e^{i\mathbf{kr}} = 1 + i\mathbf{k}\cdot\mathbf{r} - \frac{1}{2}(\mathbf{k}\cdot\mathbf{r})^2 + \cdots \tag{2}$$

is truncated after the first term. The dipole approximation is valid when $kr \ll 1$, or $\lambda \gg 2\pi r_m$ where r_m is the linear size of the molecule and λ is the radiation wavelength. Although this condition is fulfilled by applying $E_{ph} = 21.2$ eV photon energy in the present study, however the full perturbation operator Eq. (1) is applied in the calculation.

The differential cross section for the photoionization of an electron emitted into solid angle $\mathrm{d}\Omega_e$ ($\Omega_e = (\theta_e, \phi_e)$) can be written as [28]

$$\frac{\mathrm{d}\sigma}{\mathrm{d}\Omega_e} = 4\pi^2 \frac{e}{cm^2}\frac{1}{\omega_k}|\langle\Phi_{\mathbf{k}_e}|V_{int}|\Phi_i\rangle|^2 \rho(E_e = E_i + \hbar\omega_{\mathbf{k}}), \tag{3}$$

where $\Phi_{\mathbf{k}_e}$ and Φ_i denotes the ejected electron in final and initial orbitals respectively, the operator for the interaction between light and matter is given by Eq. (1) and E_i stands for the orbital binding energy. Both the initial and the final molecular orbitals (MO) are expanded over spherical harmonics around the center of mass of the molecule. $\Phi_{\mathbf{k}_e}(\mathbf{r})$ is written as

$$\Phi_{\mathbf{k}_e}(\mathbf{r}) = \frac{1}{r\sqrt{k}}\sum_{l,m} i^l e^{-i\delta_l} u_{k_e l}[Y_l^m(\hat{\mathbf{r}})]^* Y_l^m(\hat{\boldsymbol{k}}_e), \tag{4}$$

where $u_{k_e l}(r)$ is obtained from the numerical solution for the radial part of molecular Hamiltonian, $h_{\mathrm{m}} = \frac{1}{2}\Delta_{\mathrm{r}} + V_{\mathrm{m}}^+(\boldsymbol{r})$, [29]. $V_m^+(r)$ denotes the spherically averaged potential of the molecule obtained as [30]

$$V_m^+(r) = V_n(r) + V_e(r), \tag{5}$$

where the contribution of electrons is evaluated as

$$V_e(r) = -\sum_i n_i \frac{1}{4\pi}\int \mathrm{d}\boldsymbol{r}_1 \frac{|\Phi_i(\boldsymbol{r}_1)|^2}{r_>}, \qquad r_> : \max(r_1, r) \tag{6}$$

where i runs over the molecular orbitals and n_i denotes the number of electrons in the *ith* orbital. $V_n(r) = \sum_j V_{n_j}(r)$ denotes the contribution from the nuclei with

$$V_{n_j}(r) = \begin{cases} -\frac{Z_j}{R_j} & \text{if } r < R_j, \\ -\frac{Z_j}{r} & \text{if } r > R_j, \end{cases} \tag{7}$$

where Z_j stands for the nuclear charge for the jth nucleus having R_j distance from the center of mass of the molecule.

Ground state geometries and electronic structural calculations for the ground state configurations of the tetrahydrofuran molecule with C_s and C_2 symmetries are performed using density functional theory [31] incorporated in the GAUSSIAN 09 package [32]. We employed the nonlocal hybrid Becke three-parameter Lee–Yang–Parr functional (B3LYP) [33,34], and Dunning's correlation consistent polarized valence basis set of double-ζ quality (cc-pVDZ) [35]. The prominent peaks in the energy spectra of photoelectrons (PES) are identified according to their binding energy and symmetry with the help of outer valence Green's function (OVGF) calculations. Table 1 shows the results for the C_s and C_2 conformers for the ground electronic states that were considered in the present work.

4. Results

Doubly differential photoelectron spectra are presented in Fig. 2. Various bands can be observed in the energy distributions, whose intensities change almost uniformly with the observation angle. The prominent peaks in the PES can be identified according to their binding energies with the help of OVGF calculations, see Table 1. Each peak in the PES can be associated with a band of molecular orbitals at least in the outer valence region. Full Width at Half Maximum (FWHM) of the observed peaks are few tenth of eV and their broadening are due to

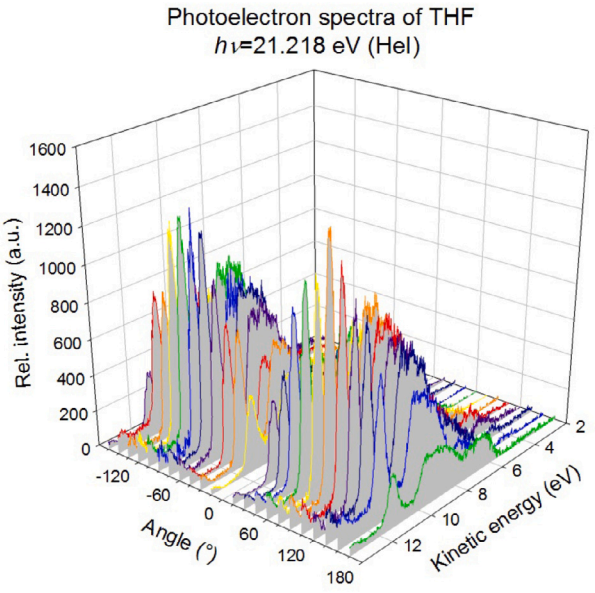

Fig. 2. Photoelectron distribution differential in ejection energy and emission angle with fixed θ_e = 90° polar angle.

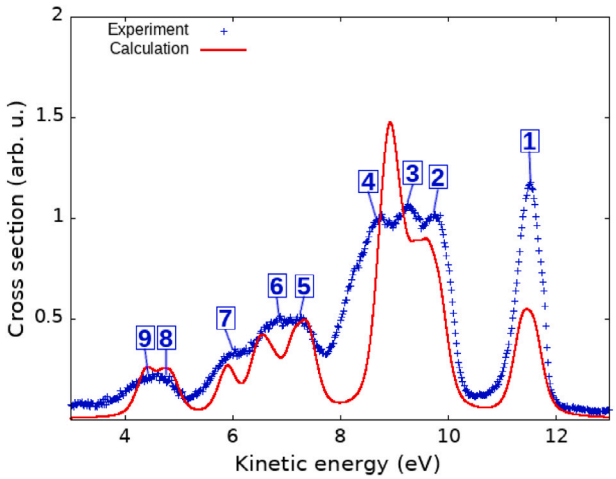

Fig. 3. Energy distribution of photolectrons. Experiment: present result (+ in blue). Present calculations: convoluted cross sections of Eq. (3) integrated over Ω_e with θ_e = 90° (red solid lines), see the text. The calculation was fitted at 8.75 eV to the experimental result for better comparison.

Table 1
Molecular orbitals and photoionization cross sections for THF. The OVGF estimates of binding energies are obtained using the cc-pVDZ basis set. CS1 is the total cross section and CS2 is the values of cross section differential in angle θ_e = 90°, see Eq. (3).

MO	Point group	OVGF (eV)	CS1 10^{-19} cm^2	CS2 10^{-19} $\frac{cm^2}{rad}$	Label used in Fig. 3
5b	C_2	−16.803	16.52	8.165	9
7a′	C_s	−16.802	16.71	9.501	9
7a	C_2	−16.488	13.01	9.119	8
8a′	C_s	−16.317	18.59	11.58	8
5a″	C_s	−15.288	32.69	18.91	7
6b	C_2	−14.773	15.57	8.627	6
8a	C_2	−14.654	31.80	18.79	6
9a′	C_s	−14.437	22.45	12.97	6
7b	C_2	−14.056	38.69	22.68	5
6a″	C_s	−13.784	50.24	29.31	5
9a	C_2	−12.419	43.12	28.08	4
10a′	C_s	−12.304	53.22	34.81	4
8b	C_2	−12.270	42.24	26.92	3
7a″	C_s	−12.188	52.39	33.04	3
10a	C_2	−12.022	41.74	22.05	3
8a″	C_s	−11.793	62.40	34.27	2
11a′	C_s	−11.564	65.58	38.09	2
11a	C_2	−11.341	56.71	33.61	2
9b	C_2	−9.820	53.34	30.50	1
12a′	C_s	−9.580	48.47	27.90	1

the Franck–Condon overlap of vibrational states. In the inner valence region satellite peaks, due to configuration interaction between quasi degenerate states with a single or multiple hole configurations in the valence region further modify the intensities and positions of the peaks.

Positions and magnitudes of the different bands can be identified much better from Fig. 3, where the PES shown in Fig. 2 integrated over the observation angle is presented. Labels of the peaks assigned to the OVGF energies are given in Table 1. The highest energy peak (band 1) is observed at E_e = 11.54 eV corresponding to E_i = −9.678 eV binding energy lying between binding energies of the 9b and 12a′ orbitals. Although the difference of binding energies between these two orbitals is ΔE = 0.24 eV their separate contributions to the peak cannot be observed due to the relatively large spot of the VUV beam used in our experiment. It has a significant influence on the present experimental resolution and unfortunately affects also the identification of the other peaks. It should also be noted that the vibrational distribution of the two ionic states can also hampers the separation of the two peaks [17,20]. Here it should be mentioned that we have to look for the possibilities for applying a more focused beam in our forthcoming studies to get a much better resolution. Three additional group of peaks can be observed in the spectrum that were dominated by bands labeled with (2, 3, 4), (5, 6, 7) and (8, 9) respectively.

Fig. 3 shows also the present theoretical result. The differential cross sections of Eq. (3) for the different E_i orbital energies are integrated over ϕ_e with θ_e = 90°. Result of this calculation is convoluted with Voigt profile that was approximated with the sum of Gaussian and Lorentzian functions given by Wertheim et al. [36]. We decided to choose 0.4 eV FWHM as it was in the best agreement with experiments. The calculated and the experimental results were normalized at 8.75 eV energy for better comparison. The convoluted results agree well with measured data on the low energy range. The theory underestimates the measured intensities by a factor of two or two and a half for band 1 and overestimates band 4 by a factor of one and a half. It cannot resolve the separate contributions of bands 3 and 4 as well. The theory predicts almost the same cross sections for orbitals that contribute to bands 3 and 4, however the differences in the orbital binding energies are small compared to the width used in the convolution.

Experimental results of Kimura et al. [37], Giuliani et al. [18] and Schmidt et al. [38] where the electrons are collected from the full angular range (not only for θ = 90° as in Fig. 3) and the corresponding theoretical calculation of the present study are presented in Fig. 4. For the sake of better comparison we normalized the different results at 8.75 eV, as in Fig. 3. Considering Figs. 3 and 4 we found that the theory presents almost the same shape for the photoelectron energy distribution integrated over the full and the restricted (θ_e = 90°) angular ranges. Regarding the measurements it can be seen that our measurements are resembles the most to the results carried out by Schmidt et al. [38]. That is the two experiments provide a very similar energy distributions. This is not the case when result of the present measurement is compared to the one of Kimura [37] and by Giuliani et al. [18]. The theoretical result differs both in the low and higher energy regions. In the outer valence region the present results predict a more pronounced decrease of cross section with decrease of E_e than that of Kimura [37] and by Giuliani et al. [18]. The first band in the measurement by Kimura et al. [37] is composed of more features in agreement with the results of Giuliani et al. [18]. The lowest energy peak corresponds to E_e = 9.433 eV binding energy, and the further peaks are attributed to vibrational excitations [18]. We must point out

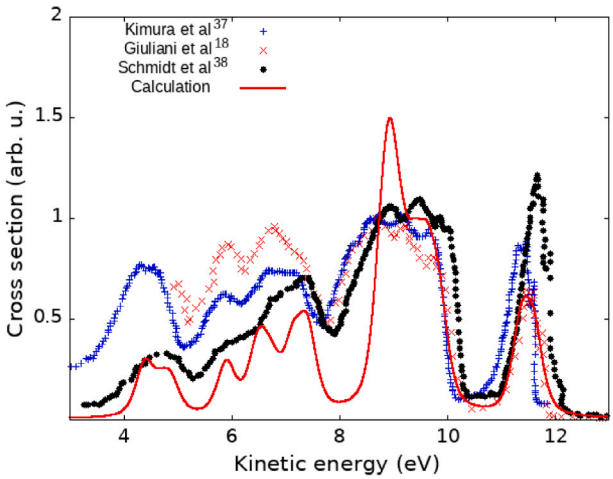

Fig. 4. Energy distribution of photoelectrons. Result of Kimura et al. [37] (+ in blue). Results of Giuliani et al. [18] (× in red). Results of Schmidt et al. [38] (· in black). Present calculations: convoluted cross sections of Eq. (3) integrated over Ω_e (red solid lines). The different results were normalized at 8.75 eV.

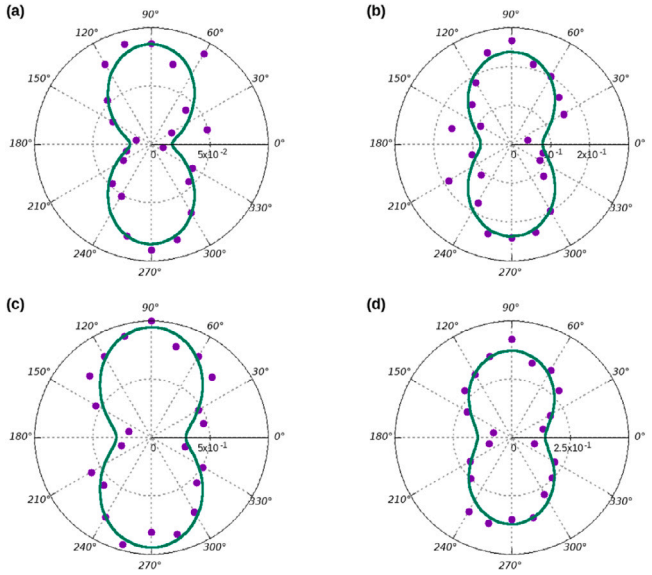

Fig. 5. Angular distribution of photoelectrons corresponding to bands 8–9 (a); 5–7 (b); 2–4 (c) and 1 (d) depicted in Fig. 3. Dots: present measurement. Lines: present calculation.

that the experiments performed by different groups [18,37,38] significantly differ from each other and our measurements are in the best agreement with the measurements performed by Schmidt et al. [38].

One of the main advantages of the ESA-22 spectrometer is that it allows the measurements of the photoelectrons to the full 4π angular region. However, as it is noted above the present measurement was performed only at one given polar emission angle ($\theta_e = 90°$), namely we measured the electron distribution in the x-z plane. The recorded angular distributions of photoelectrons for some ejection energies are presented in Fig. 5. The presented four angular distributions were measured in a limited energy range corresponding to bands 1, 2–4, 5–7 and 8–9 depicted in Fig. 3. Good agreement can be observed between the measured and calculated data. However, it should be noted that the uncertainty of experimental data increase with the decrease of energy of the emitted electrons as the absolute detector efficiencies are decreasing with the measured electron energy depicted by Ábrók et al. [27]. We can conclude that the dipole transition dominates

Table 2
The β asymmetry parameters for different energies.

Corresponding bands	β		
	Experiment	Error	Theory
8–9	1.200	0.180	1.112
5–7	0.781	0.139	0.795
2–4	0.772	0.088	0.839
1	0.893	0.086	0.689

the transition in the whole ejection energy region considered. This is supported by the theoretical calculations, where the contributions of non-dipole terms were less than 0.1%. In dipole approximation the angular distribution can be described by the β asymmetry parameter defined as $\frac{d\sigma}{d\Omega_e} = \frac{\sigma_0}{4\pi}[1 + \beta P_2(cos\theta)]$ [39], where σ_0 is the total cross section and P_2 is the Legendre polynomial of second order. The β parameters can be obtained by fitting the experimental and calculated data with the above formula. Table 2 shows the β parameters for different bands.

Our future goal is to measure the full 3D angular distribution of the photoelectrons measured from tetrahydrofuran that can be achieved with the rotation of the spectrometer. This aim will be supported by using Position Sensitive Detector (PSD) instead of CEMs, see the electron trajectories on the right side in Fig. 1. By employing PSD, measurement times can significantly be reduced compared to CEMs as PSD is capable of measuring an energy interval simultaneously in contrast to the CEMs. This method also enables us to measure more detailed angular distribution.

5. Conclusion

In this paper we present a measurement for the energy and angular distributions of the photoionised electrons from tetrahydrofuran using a vacuum ultraviolet photon source. We were the first group having measured the angular distribution from THF in the 0°–360° angular region and determined the β asymmetry parameters. Numerical calculations are also performed to study the process. Bands in the energy distributions of the emitted electrons are identified using binding energies provided by the OVGF method. Except for bands 1 and 4 the measured photoelectron intensities are in reasonable agreement with the calculated ones.

The present experimental energy distribution, obtained on a limited angular region ($\theta_e = 90°$), is compared with the results of other groups [18,37,38] corresponding to the whole angular emission range. Our experimental result is in the best agreement with the one carried out by Schmidt et al. [38]. Measurements by Kimura and Giuliani et al. [18,37] reveal more fine details in the structure of the different bands. Interestingly, the calculation also overestimates the measured by Schmidt et al. [38] for band 4 and underestimates for band 1. The same can be concluded regarding our experimental result and calculation obtained on limited angular range.

The observed angular distributions reveal the character of dipole transition in the whole electron ejection energy range in agreement with the theoretical calculation. In order to improve experimental resolutions both for the energy and the angular distribution, a more focused photon beam will be required in our further experimental studies.

Acknowledgments

The authors thank Dezső Varga for discussions on the measurements. This work was supported by the Hungarian Scientific Research Fund (Grant No. K128621) and the National Research, Development and Innovation Office, Hungary (Grant No. 2018-1.2.1-NKP-2018-00010) and the National Information Infrastructure Development Program, Hungary.

References

[1] M.A. Huels, I. Hahndorf, E. Illenberger, L. Sanche, Resonant dissociation of DNA bases by subionization electrons, J. Chem. Phys. 108 (4) (1998) 1309–1312, http://dx.doi.org/10.1063/1.475503.

[2] G. Hanel, B. Gstir, S. Denifl, P. Scheier, M. Probst, B. Farizon, M. Farizon, E. Illenberger, T.D. Märk, Electron attachment to uracil: Effective destruction at subexcitation energies, Phys. Rev. Lett. 90 (18) (2003) 4, http://dx.doi.org/10.1103/PhysRevLett.90.188104.

[3] M. Takeshita, C.N. Chang, F. Johnson, S. Will, A.P. Grollman, Oligodeoxynucleotides containing synthetic abasic sites. Model substrates for DNA polymerases and apurinic/apyrimidinic endonucleases, J. Biol. Chem. 262 (21) (1987) 10171–10179, http://dx.doi.org/10.1016/S0021-9258(18)61093-2.

[4] S. Tonzani, C.H. Greene, Radiation damage to DNA: Electron scattering from the backbone subunits, J. Chem. Phys. 125 (9) (2006) 094504, http://dx.doi.org/10.1063/1.2333455.

[5] E. Erdmann, M.-C. Bacchus-Montabonel, M. Łabuda, Modelling charge transfer processes in C2+–tetrahydrofuran collision for ion-induced radiation damage in DNA building blocks, Phys. Chem. Chem. Phys. 19 (2017) 19722–19732, http://dx.doi.org/10.1039/C7CP02100C.

[6] A. Zecca, C. Perazzolli, M.J. Brunger, Positron and electron scattering from tetrahydrofuran, J. Phys. B: At. Mol. Opt. Phys. 38 (13) (2005) 2079–2086, http://dx.doi.org/10.1088/0953-4075/38/13/002.

[7] M. Allan, Absolute angle-differential elastic and vibrational excitation cross sections for electron collisions with tetrahydrofuran, J. Phys. B: At. Mol. Opt. Phys. 40 (17) (2007) 3531–3544, http://dx.doi.org/10.1088/0953-4075/40/17/020.

[8] C.J. Colyer, S.M. Bellm, B. Lohmann, G.F. Hanne, O. Al-Hagan, D.H. Madison, C.G. Ning, Dynamical (e, 2e) studies using tetrahydrofuran as a DNA analog, J. Chem. Phys. 133 (12) (2010) 124302, http://dx.doi.org/10.1063/1.3491030.

[9] M. Dampc, I. Linert, A.R. Milosavljević, M. Zubek, Vibrational excitation of tetrahydrofuran by electron impact in the low energy range, Chem. Phys. Lett. 443 (1) (2007) 17–21, http://dx.doi.org/10.1016/j.cplett.2007.06.048.

[10] M. Dampc, E. Szymańska, B. Mielewska, M. Zubek, Ionization and ionic fragmentation of tetrahydrofuran molecules by electron collisions, J. Phys. B: At. Mol. Opt. Phys. 44 (5) (2011) 055206, http://dx.doi.org/10.1088/0953-4075/44/5/055206.

[11] T.P.T. Do, M. Leung, M. Fuss, G. Garcia, F. Blanco, K. Ratnavelu, M.J. Brunger, Excitation of electronic states in tetrahydrofuran by electron impact, J. Chem. Phys. 134 (14) (2011) 144302, http://dx.doi.org/10.1063/1.3575454.

[12] D. Duflot, J.-P. Flament, A. Giuliani, J. Heinesch, M.-J. Hubin-Franskin, Ab initio and experimental study of the K-shell spectra of 2,5-dihydrofuran, Chem. Phys. 310 (1) (2005) 67–75, http://dx.doi.org/10.1016/j.chemphys.2004.10.007.

[13] D. Duflot, J.-P. Flament, J. Heinesch, M.-J. Hubin-Franskin, The K-shell spectra of tetrahydrofuran studied by electron energy loss spectroscopy and abinitio calculations, Chem. Phys. Lett. 495 (1) (2010) 27–32, http://dx.doi.org/10.1016/j.cplett.2010.06.058.

[14] M. Fuss, A. Muñoz, J.C. Oller, F. Blanco, D. Almeida, P. Limão Vieira, T.P.D. Do, M.J. Brunger, G. García, Electron-scattering cross sections for collisions with tetrahydrofuran from 50 to 5000 eV, Phys. Rev. A 80 (2009) 052709, http://dx.doi.org/10.1103/PhysRevA.80.052709.

[15] D. Jones, J. Builth-Williams, S. Bellm, L. Chiari, H. Chaluvadi, D. Madison, C. Ning, B. Lohmann, O. Ingólfsson, M. Brunger, Dynamical (e,2e) investigations of tetrahydrofuran and tetrahydrofurfuryl alcohol as DNA analogues, Chem. Phys. Lett. 572 (2013) 32–37, http://dx.doi.org/10.1016/j.cplett.2013.04.028.

[16] C.G. Ning, Y.R. Huang, S.F. Zhang, J.K. Deng, K. Liu, Z.H. Luo, F. Wang, Experimental and theoretical electron momentum spectroscopic study of the valence electronic structure of tetrahydrofuran under pseudorotation, J. Phys. Chem. A 112 (2008) 11078–11087, http://dx.doi.org/10.1021/jp8038658.

[17] M. Dampc, B. Mielewska, M.R. Siggel-King, G.C. King, M. Zubek, Threshold photoelectron spectra of tetrahydrofuran over the energy range 9-29 eV, Chem. Phys. 359 (1) (2009) 77–81, http://dx.doi.org/10.1016/j.chemphys.2009.03.009.

[18] A. Giuliani, P. Limão-Vieira, D. Duflot, A.R. Milosavljevic, B.P. Marinkovic, S.V. Hoffmann, N. Mason, J. Delwiche, M.-J. Hubin-Franskin, Electronic states of neutral and ionized tetrahydrofuran studied by vuv spectroscopy and ab initio calculations, Eur. Phys. J. D 51 (1) (2009) 97–108, http://dx.doi.org/10.1140/epjd/e2008-00154-7.

[19] M.G.P. Homem, P. Iza, L.S. Farenzena, R.L. Cavasso-Filho, M.T. Lee, I. Iga, Cross-section measurements of photoabsorption and ionization quantum yields for tetrahydrofuran in the vacuum-ultraviolet energy range, J. Phys. B: At. Mol. Opt. Phys. 42 (23) (2009) 235204, http://dx.doi.org/10.1088/0953-4075/42/23/235204.

[20] P.M. Mayer, M.F. Guest, L. Cooper, L.G. Shpinkova, E.E. Rennie, D.M.P. Holland, D.A. Shaw, Does tetrahydrofuran ring open upon ionization and dissociation? A tpes and TPEPICO investigation, J. Phys. Chem. A 113 (41) (2009) 10923–10932, http://dx.doi.org/10.1021/jp906440p, PMID: 19775111.

[21] S.H.R. Shojaei, F. Morini, M.S. Deleuze, Photoelectron and electron momentum spectroscopy of tetrahydrofuran from a molecular dynamical perspective, J. Phys. Chem. A 117 (9) (2013) 1918–1929, http://dx.doi.org/10.1021/jp310722a, PMID: 23387306.

[22] R.M. Young, M.A. Yandell, M. Niemeyer, D.M. Neumark, Photoelectron imaging of tetrahydrofuran cluster anions $[(THF)_n^-]$ $(1 \leqslant n \leqslant 100)$, J. Chem. Phys. 133 (15) (2010) 154312, http://dx.doi.org/10.1063/1.3489686.

[23] B. Boudaïffa, P. Cloutier, D. Hunting, M.A. Huels, L. Sanche, Resonant formation of DNA strand breaks by low-energy (3 to 20 ev) electrons, Science 287 (5458) (2000) 1658–1660, http://dx.doi.org/10.1126/science.287.5458.1658.

[24] B. Cadioli, E. Gallinella, C. Coulombeau, H. Jobic, G. Berthier, Geometric structure and vibrational spectrum of tetrahydrofuran, J. Phys. Chem. 97 (30) (1993) 7844–7856, http://dx.doi.org/10.1021/j100132a010.

[25] V.c. Rayón, J. Sordo, Pseudorotation motion in tetrahydrofuran: An ab initio study, J. Chem. Phys. 122 (2005) 204303, http://dx.doi.org/10.1063/1.1899123.

[26] T. Yang, G. Su, C. Ning, J. Deng, F. Wang, S. Zhang, X. Ren, Y. Huang, New diagnostic of the most populated conformer of tetrahydrofuran in the gas phase, J. Phys. Chem. A 111 (23) (2007) 4927–4933, http://dx.doi.org/10.1021/jp066299a, PMID: 17511427.

[27] L. Ábrók, T. Buhr, A. Kövér, R. Balog, D. Hatvani, P. Herczku, S. Kovács, S. Ricz, A method for intensity calibration of an electron spectrometer with multi-angle detection, Nucl. Instrum. Methods Phys. Res. B 369 (2016) 24–28, http://dx.doi.org/10.1016/j.nimb.2015.10.037, Photon and fast Ion induced Processes in Atoms, Molecules and Nanostructures (PIPAMON).

[28] M. Weissbluth, Atoms and Molecules, Academic Press, Inc., New York, 1978.

[29] L. Gulyás, P.D. Fainstein, A. Salin, CDW-EIS theory of ionization by ion impact with Hartree-Fock description of the target, J. Phys. B: At. Mol. Opt. Phys. 28 (1995) 245, http://dx.doi.org/10.1088/0953-4075/28/2/013.

[30] L. Gulyás, I. Tóth, L. Nagy, CDW-EIS calculation for ionization and fragmentation of methane impacted by fast protons, J. Phys. B: At. Mol. Opt. Phys. 46 (2013) 075201, http://dx.doi.org/10.1088/0953-4075/46/7/075201.

[31] R.M. Dreizler, E.K.U. Gross, Density Functional Theory, Springer-Verlag, Berlin, 1990.

[32] M.J. Frisch, G.W. Trucks, H.B. Schlegel, G.E. Scuseria, M.A. Robb, J.R. Cheeseman, G. Scalmani, V. Barone, B. Mennucci, G.A. Petersson, H. Nakatsuji, M. Caricato, X. Li, H.P. Hratchian, A.F. Izmaylov, J. Bloino, G. Zheng, J.L. Sonnenberg, M. Hada, M. Ehara, K. Toyota, R. Fukuda, J. Hasegawa, M. Ishida, T. Nakajima, Y. Honda, O. Kitao, H. Nakai, T. Vreven, J.A. Montgomery, J.E. Peralta, F. Ogliaro, M. Bearpark, J.J. Heyd, E. Brothers, K.N. Kudin, V.N. Staroverov, R. Kobayashi, J. Normand, K. Raghavachari, A. Rendell, J.C. Burant, S.S. Iyengar, J. Tomasi, M. Cossi, N. Rega, J.M. Millam, M. Klene, J.E. Knox, J.B. Cross, V. Bakken, C. Adamo, J. Jaramillo, R. Gomperts, R.E. Stratmann, O. Yazyev, A.J. Austin, R. Cammi, C. Pomelli, J.W. Ochterski, R.L. Martin, K. Morokuma, V.G. Zakrzewski, G.A. Voth, P. Salvador, J.J. Dannenberg, S. Dapprich, A.D. Daniels, Farkas, J.B. Foresman, J.V. Ortiz, J. Cioslowski, D.J. Fox, Gaussian 09 Revision E.01, Gaussian Inc. Wallingford CT, 2009.

[33] A.D. Becke, Density-functional thermochemistry. III. The role of exact exchange, J. Chem. Phys. 98 (7) (1993) 5648–5652, http://dx.doi.org/10.1063/1.464913.

[34] C. Lee, W. Yang, R.G. Parr, Development of the Colle-Salvetti correlation-energy formula into a functional of the electron density, Phys. Rev. B 37 (1988) 785–789, http://dx.doi.org/10.1103/PhysRevB.37.785.

[35] T.H. Dunning, Gaussian basis sets for use in correlated molecular calculations. I. The atoms boron through neon and hydrogen, J. Chem. Phys. 90 (2) (1989) 1007–1023, http://dx.doi.org/10.1063/1.456153.

[36] G.K. Wertheim, M.A. Butler, K.W. West, D.N.E. Buchanan, Determination of the Gaussian and Lorentzian content of experimental line shapes, Rev. Sci. Instrum. 45 (11) (1974) 1369–1371, http://dx.doi.org/10.1063/1.1686503.

[37] K. Kimura, S. Katsumata, Y. Achiba, T. Yamazaki, S. Iwata, Handbook of HeI Photoelectron Spectra of Fundamental Organic Molecules: Ionization Energies, Ab Initio Assignments and Valence Elcetronic Structure for 200 Molecules, Japan Scientific Societies Press, 1981.

[38] H. Schmidt, A. Schweig, Notiz zur transanularen n/π -Wechselwirkung in 2,5-Dihydrofuran, Chem. Berichte 107 (2) (1974) 725–726, http://dx.doi.org/10.1002/cber.19741070249.

[39] J.W. Cooper, Photoelectron-angular-distribution parameters for rare-gas subshells, Phys. Rev. A 47 (1993) 1841–1851, http://dx.doi.org/10.1103/PhysRevA.47.1841.